Detecting invariant manifolds as stationary Lagrangian coherent structures in autonomous dynamical systems

Hiroshi Teramoto, George Haller, and Tamiki Komatsuzaki

Citation: Chaos: An Interdisciplinary Journal of Nonlinear Science **23**, 043107 (2013); doi: 10.1063/1.4824314
View online: http://dx.doi.org/10.1063/1.4824314
View Table of Contents: http://scitation.aip.org/content/aip/journal/chaos/23/4?ver=pdfcov
Published by the AIP Publishing

Detecting invariant manifolds as stationary Lagrangian coherent structures in autonomous dynamical systems

Hiroshi Teramoto,[1,a)] George Haller,[2] and Tamiki Komatsuzaki[1]
[1]*Molecule & Life Nonlinear Sciences Laboratory, Research Institute for Electronic Science, Hokkaido University, Kita 20 Nishi 10, Kita-ku, Sapporo 001-0020, Japan*
[2]*Institute for Mechanical Systems, ETH Zürich, CLA J.27, Tannenstrasse 3, 8092 Zürich, Switzerland*

(Received 8 April 2013; accepted 23 September 2013; published online 16 October 2013)

Normally hyperbolic invariant manifolds (NHIMs) are well-known organizing centers of the dynamics in the phase space of a nonlinear system. Locating such manifolds in systems far from symmetric or integrable, however, has been an outstanding challenge. Here, we develop an automated detection method for codimension-one NHIMs in autonomous dynamical systems. Our method utilizes Stationary Lagrangian Coherent Structures (SLCSs), which are hypersurfaces satisfying one of the necessary conditions of a hyperbolic LCS, and are also quasi-invariant in a well-defined sense. Computing SLCSs provides a quick way to uncover NHIMs with high accuracy. As an illustration, we use SLCSs to locate two-dimensional stable and unstable manifolds of hyperbolic periodic orbits in the classic ABC flow, a three-dimensional solution of the steady Euler equations. © *2013 AIP Publishing LLC*. [http://dx.doi.org/10.1063/1.4824314]

Invariant manifolds play an important role in transport phenomena that range from chemical reactions through fluid mixing to celestial mechanics. Such manifolds, however, are often challenging to locate in multi-dimensional systems that are far from integrable and possess no special symmetries. Among these invariant manifolds, normally hyperbolic invariant manifolds are particularly important due to their persistence under small perturbations. This renders them robust with respect to modeling errors and numerical inaccuracies. Here, we develop a method to detect codimension-one, normally hyperbolic invariant manifolds in general autonomous systems. We approximate such manifolds as zero level sets of a scalar function derived from the recent variational theory of hyperbolic Lagrangian Coherent Structures (LCSs). This approximation converges exponentially fast to a true invariant manifold as longer and longer flow-map samples are used in its construction. We illustrate this method on the classic steady ABC flow, revealing some of its two-dimensional invariant manifolds at a previously unseen level of detail.

I. INTRODUCTION

Normally hyperbolic invariant manifolds (NHIMs) are surfaces that act as organizing centers in the phase space of a dynamical system. Such manifolds have normal attraction and repulsion rates that dominate their tangential contraction and stretching rates, respectively. This property renders compact NHIMs both smooth and persistent under small perturbations (Hirsch *et al.*,[1,2] and Fenichel[3]), which in turn makes them important in a number of applications (see, e.g., Refs. 4–6).

Despite their significance, neither the theoretical framework of Hirsch *et al.*[1,2] nor that of Fenichel[3] provide a way to actually locate NHIMs, which therefore have remained notoriously difficult to detect in multi-dimensional dynamical systems. Unless the dynamical system is close to an integrable system with an explicitly known NHIMs (Haller[6]), has two vastly different time scales (Jones[5]), or suggests a first guess for the rough location of a NHIM (Broer *et al.*,[7] Capinski and Simó[8]), one has little chance to locate NHIMs without extensive numerical experimentation.

The most important NHIMs are codimension-one manifolds (hypersurfaces), which locally partition the phase space into two non-interacting regions. Examples include normally hyperbolic subsets of stable and unstable manifolds of codimension-two hyperbolic invariant sets, such as codimension-two tori. Codimension-one NHIMs have a decisive impact on trajectories through the exponential attraction or repulsion that they exhibit in their single normal direction. As a result, codimension-one NHIMs act as observed attractors for all nearby tracer trajectories in forward and backward time. This is a property they share with Lagrangian Coherent Structures (LCSs), which are locally most attracting or repelling material surfaces over a fixed finite time interval (Haller and Yuan,[9] Haller[10]).

A material surface is a time-dependent, codimension-one manifold of initial conditions that evolves under the flow map. Accordingly, an LCS is an invariant manifold in the extended phase space of the phase space variables and time. However, an LCS is generally not an invariant manifold in the phase space itself, even if the underlying dynamical system is autonomous. Accordingly, an LCS is generally a time-dependent hypersurface, observed as the *de facto* attractor for all nearby initial conditions in forward or backward time over the finite time-interval involved in its definition. Therefore, an LCS is only guaranteed to be invariant in the extended phase space, even if the underlying dynamical system is autonomous.

The theory of LCSs has only recently reached a level of maturity comparable to that of NHIMs. Specifically, the

a)teramoto@es.hokudai.ac.jp

variational theory of hyperbolic LCSs developed in Haller[10] and Farazmand and Haller[11] now offers a rigorous set of computable criteria for detecting LCSs globally in the phase space in an automated fashion. Early ideas on constraining such variationally constructed LCSs to be nearly invariant manifolds appear in Haller.[10] The constrained approach presented there, however, only applies to two-dimensional autonomous systems, or to LCSs that are codimension-one level sets of an conserved quantity. In particular, no related results have been available for systems without conserved quantities, or for codimension-one LCSs within the energy surface of an autonomous Hamiltonian system. Clearly, locating NHIMs with the help of LCSs in the latter two classes of flows is of great importance in applications, including steady three-dimensional fluid flows and multi-dimensional autonomous Hamiltonian systems of classical mechanics.

Here, we develop a new approach that detects NHIMs as constrained LCSs in dynamical systems of arbitrary dimension. Our approach requires no assumption on near-integrability, time-scale separation, or a rough knowledge of the location of the NHIM. As a result, the method developed here is suitable for the automated exploration of codimension-one NHIMs in any finite-dimensional, autonomous dynamical system.

We approximate such NHIMs via Stationary LCSs (SLCSs), which are hypersurfaces satisfying a necessary condition for a hyperbolic LCS, while also showing a high degree of invariance (quasi-invariance) in the phase space. The necessary LCS condition simply requires orthogonality between the vector field generating the dynamical system and the dominant eigenvector field of the Cauchy-Green strain tensor computed from the flow map. This orthogonality generically holds along a union of codimension-one surfaces, computed as the zero set of the inner product of the two vector fields involved. The quasi-invariance condition then identifies subsets of this zero surface that are nearly invariant. If quasi-invariance is enforced at a high enough level, the SLCSs obtained in this fashion are numerically indistinguishable from actual NHIMs.

This paper is organized as follows. In Sec. II, we develop the necessary notation and terminology, and in Sec. III, we review the relevant mathematical concepts from the variational theory of hyperbolic LCSs. In Sec. IV, we develop the concept of SLCSs, and relate it to codimension-one NHIMs in Sec. V. In Sec. VI, we present a simple algorithm for the global construction of SLCSs in autonomous dynamical systems, with an application to the three-dimensional ABC flow shown in Sec. VII. We give a summary and outlook in Sec. VIII.

II. SET-UP AND NOTATION

Let X be a C^r-vector flow ($r \geq 2$) defined on $\mathbb{R}^n$ and ϕ^t be the corresponding flow, i.e.,$\phi^t(\mathbf{z})$ is the position at time $t\,(-T \leq t \leq T)$ starting from $\mathbf{z}$ at time 0, where $\mathbf{z} = (z_1, \cdots, z_n)$ and $\phi^t(\mathbf{z}) = (\phi_1^t(\mathbf{z}), \ldots, \phi_n^t(\mathbf{z}))$. If the vector field does not depend on the time explicitly, the position does not depend on the starting time. Let $X(\mathbf{z})$ be the vector fields at the position $\mathbf{z}$, $X(\mathbf{z}) = (X_1(\mathbf{z}), \ldots, X_n(\mathbf{z}))$. In terms of the vector fields, the time evolution equation of the system can be written as

$$\frac{d\phi^t(\mathbf{z})}{dt} = X\left(\phi^t(\mathbf{z})\right). \tag{1}$$

The dynamics in the vicinity of the trajectory can be understood in terms of the differential of the flow (linearized flow map),

$$D\phi^t(\mathbf{z}) = \begin{pmatrix} \frac{\partial \phi_1^t(\mathbf{z})}{\partial z_1} & \cdots & \frac{\partial \phi_1^t(\mathbf{z})}{\partial z_n} \\ \vdots & \ddots & \vdots \\ \frac{\partial \phi_n^t(\mathbf{z})}{\partial z_1} & \cdots & \frac{\partial \phi_n^t(\mathbf{z})}{\partial z_n} \end{pmatrix}. \tag{2}$$

This differential obeys the following time evolutional equation:

$$\frac{d}{dt} D\phi^t(\mathbf{z}) = \frac{\partial X(\mathbf{z}')}{\partial \mathbf{z}'} D\phi^t(\mathbf{z}), \tag{3}$$

where $\mathbf{z}' = \phi^t(\mathbf{z})$ and

$$\frac{\partial X(\mathbf{z})}{\partial \mathbf{z}} = \begin{pmatrix} \frac{\partial X_1(\mathbf{z})}{\partial z_1} & \cdots & \frac{\partial X_1(\mathbf{z})}{\partial z_n} \\ \vdots & \ddots & \vdots \\ \frac{\partial X_n(\mathbf{z})}{\partial z_1} & \cdots & \frac{\partial X_n(\mathbf{z})}{\partial z_n} \end{pmatrix}. \tag{4}$$

Using the differential of the flow (Eq. (2)), the Cauchy-Green strain tensor can be calculated as $C^T(\mathbf{z}) = (D\phi^T(\mathbf{z}))^* D\phi^T(\mathbf{z})$ where $(D\phi^T(\mathbf{z}))^*$ is the transpose of $D\phi^T(\mathbf{z})$. These eigenvalues and eigenvectors are denoted by $c_i^T(\mathbf{z})\,(1 \leq i \leq n)$ and $\xi_i^T(\mathbf{z}) = (\xi_{i1}^T(\mathbf{z}), \ldots, \xi_{in}^T(\mathbf{z}))\,(1 \leq i \leq n)$, respectively, and satisfies $C^T(\mathbf{z})\xi_i^T(\mathbf{z}) = c_i^T(\mathbf{z})\xi_i^T(\mathbf{z})\,(1 \leq i \leq n)$. Here, the eigenvalues are indexed in ascending order such that $c_1^T(\mathbf{z}) \leq c_2^T(\mathbf{z}) \leq \cdots \leq c_{n-1}^T(\mathbf{z}) \leq c_n^T(\mathbf{z})$ and the eigenvectors are normalized such that $\xi_i^T(\mathbf{z}) \cdot \xi_j^T(\mathbf{z}) = \delta_{ij}\,(1 \leq i,j \leq n)$ where δ_{ij} denotes the Kronecker delta (note that the eigenvectors are orthogonal to each other because the Cauchy-Green strain tensor is symmetric). Each eigenvector spans a linear 1-dimensional vector space $E_{\mathbf{z},i}^T\,(1 \leq i \leq n)$. In terms of the vector spaces, the ambient vector space $T_{\mathbf{z}}\mathbb{R}^n$ can be decomposed as $T_{\mathbf{z}}\mathbb{R}^n = \oplus_{i=1}^n E_{\mathbf{z},i}^T$. The physical meaning of $c_i^T(\mathbf{z})\,(i = 1, \ldots, n)$ and $\xi_i^T(\mathbf{z})\,(i = 1, \ldots, n)$ is as follows: If the initial condition $\mathbf{z}$ is infinitesimally displaced in the $\xi_i^T(\mathbf{z})$ direction, the displacement results in $D\phi^T(\mathbf{z})\xi_i^T(\mathbf{z})$ after time T. In terms of the Euclidean metric, the length of the vector is

$$\begin{aligned} \|D\phi^T(\mathbf{z})\xi_i^T(\mathbf{z})\| &= \sqrt{\left(D\phi^T(\mathbf{z})\xi_i^T(\mathbf{z})\right) \cdot D\phi^T(\mathbf{z})\xi_i^T(\mathbf{z})}, \\ &= \sqrt{\xi_i^T(\mathbf{z})^* \left(D\phi^T(\mathbf{z})\right)^* D\phi^T(\mathbf{z})\xi_i^T(\mathbf{z})}, \\ &= \sqrt{\xi_i^T(\mathbf{z})^* C^T(\mathbf{z})\xi_i^T(\mathbf{z})}, \\ &= \sqrt{c_i^T(\mathbf{z})}. \end{aligned} \tag{5}$$

Therefore, the displacement along $\xi_i^T(\mathbf{z})$ is magnified $\sqrt{c_i^T(\mathbf{z})}$ times in the Euclidean metric. Specifically, the largest eigenvectors can be characterized in a variational manner such that

$$\|D\phi^T(\mathbf{z})\| = \max_{v \in T_{\mathbf{z}}\mathbb{R}^n} \frac{\|D\phi^T(\mathbf{z})v\|}{\|v\|} = \|D\phi^T(\mathbf{z})\xi_n^T(\mathbf{z})\|, \quad (6)$$

i.e., $\xi_n^T(\mathbf{z})$ is a direction of maximal stretching.

III. A BRIEF REVIEW OF HYPERBOLIC LCS

A Lagrangian Coherent Structure (LCS), as defined originally by Haller and Yuan,[9] is a codimension-one material surface that is locally the most repelling or attracting among C^1-close material surfaces over a given finite time interval $[0, T]$. Here, the definition of the material surface is the following.

Definition III.1 (Material Surface). A material surface $\mathcal{M}(t) \subset \mathbb{R}^n$ over the time interval [0, T] is a surface that satisfies $\phi^t(\mathcal{M}(0)) = \mathcal{M}(t)$ for all $t \in [0, T]$.

As shown in Haller,[10] such a material surface can be identified based on the following theorem:

Theorem III.1 (LCS). *An (n – 1)-dimensional surface $\mathcal{M}_{\mathrm{LCS}}(t) \subset \mathbb{R}^n$ is a repelling LCS over the time interval [0, T] if and only if:*

I. $\mathcal{M}_{\mathrm{LCS}}(t)$ is a material surface over the time interval $[0, T]$.
II. Each point of $\mathcal{M}_{\mathrm{LCS}}(t)$ admits a unique direction of maximal stretching: $c_{n-1}^T(\mathbf{z}) < c_n^T(\mathbf{z})$ and $c_n^T(\mathbf{z}) > 1$ hold for every $\mathbf{z} \in \mathcal{M}_{\mathrm{LCS}}(0)$.
III. This maximal stretching direction, $\xi_n^T(\mathbf{z})$, is normal to $\mathcal{M}_{\mathrm{LCS}}(0)$.
IV. The normal repulsion rate of $\mathcal{M}_{LCS}(t)$ is maximal relative to those of nearby material surfaces (cf. Haller[10] and Farazmand and Haller[11] for details).

As argued in Farazmand and Haller,[11] condition IV of Theorem III.1 turns out to be somewhat restrictive in that it requires the LCS to be the most repelling among all nearby material surfaces. Apart from a few idealized examples, such a strong extremum property will not be achieved by material surfaces over finite time intervals (see, e.g., Appendix B for a simple example of a stable manifold that is not a locally most repelling material surface).

For this reason, Farazmand and Haller[11] give a relaxed formulation for two-dimensional flows. In this formulation, condition IV is replaced with a weaker requirement that the average stretching on the LCS is maximal relative to all nearby material surfaces that satisfy condition III, i.e., are pointwise normal to the dominant eigenvector of the Cauchy-Green strain tensor.

IV. DEFINITION AND PROPERTIES OF AN SLCS

To detect NHIMs as LCSs, a weaker form of condition III of Theorem III.1 turns out to be useful. Accordingly, in our definition of a Stationary LCS (SLCS) below, we keep conditions I–II of Theorem III.1, and require trajectories in the SLCS (as opposed to the whole tangent space of the SLCS) to be orthogonal to the direction of largest stretching, and also require this largest stretching direction to be close to the normal of the SLCS.

Definition IV.1 (SLCS). $\mathcal{M}$ is a repelling SLCS of a finite time duration $T > 0$ and tolerances $\epsilon \in [0, 1)$ and $\alpha \in [0, \pi/2]$ if $\mathcal{M}$ satisfies the following three properties. For every $\mathbf{z} \in \mathcal{M}$,

A. $L^T(\mathbf{z}) \equiv \xi_n^T(\mathbf{z}) \cdot X(\mathbf{z}) = 0$.
B. $c_{n-1}^T(\mathbf{z}) < \epsilon^2 c_n^T(\mathbf{z})$ and $c_n^T(\mathbf{z}) > 1$.
C. $|\cos^{-1}(|\xi_n^T(\mathbf{z}) \cdot \mathbf{n}(\mathbf{z})|)| \le \alpha$,

where $\mathbf{n}(\mathbf{z})$ is a unit normal vector to $\mathcal{M}$ at $\mathbf{z} \in \mathcal{M}$.

The schematic geometry of an SLCS is shown in Fig. 1. An attracting SLCS can be defined analogously as a repelling SLCS in backward time ($T < 0$).

Remark IV.1.1: The parameter ϵ in Definition IV.1 controls the required spectral gap between the two largest eigenvalues of the Cauchy-Green strain tensor. The smaller ϵ, the more the rate of repulsion normal to the SLCS dominates the largest stretching rate within the SLCS. The parameter α controls the degree to what extent the SLCS is required to be invariant (note that $\alpha = 0$ corresponds to full invariance).

Remark IV.1.2: Condition A is a necessary condition for the SLCS to be an LCS, requiring that the trajectory through any point of the SLCS be normal to the direction of largest strain $\xi_n^T(\mathbf{z})$ at that point. Note that this condition is necessary but not sufficient for the SLCS to be normal to the direction of largest strain.

Remark IV.1.3: Condition B for SLCS is stronger than condition II for LCS. Selecting ϵ small enough for an SLCS will ensure small variation of the SLCS under changes in the detection interval length T. Specifically, note that (see Appendix A for a proof),

$$\left\| \frac{d\xi_n^T(\mathbf{z})}{dT} \right\| \le \frac{\sqrt{n-1}G\epsilon}{1-\epsilon^2}, \quad (7)$$

where

$$G = \sup_{\mathbf{z}' \in \mathbb{R}^n} \left\| \frac{\partial X(\mathbf{z}')^*}{\partial \mathbf{z}'} + \frac{\partial X(\mathbf{z}')}{\partial \mathbf{z}'} \right\|. \quad (8)$$

Therefore,

$$\left| \frac{dL^T(\mathbf{z})}{dT} \right| \le \left\| \frac{d\xi_n^T(\mathbf{z})}{dT} \right\| \|X(\mathbf{z})\| \le \frac{\sqrt{n-1}G\epsilon}{1-\epsilon^2} \|X(\mathbf{z})\|. \quad (9)$$

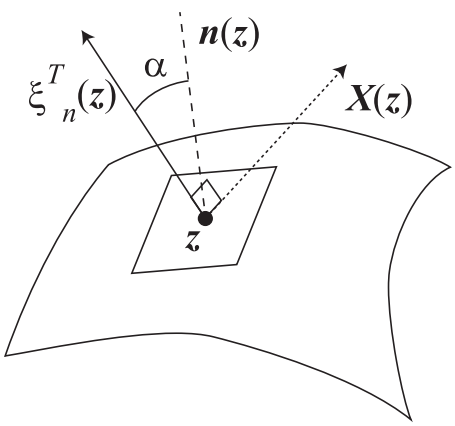

FIG. 1. A schematic figure of SLCS.

This means that fluctuations in the value of $L^T(\mathbf{z})$ is of order ϵ.

Under conditions B and C, the flux across the LCS (and hence the degree of invariance of the LCS) can be estimated as follows.

Theorem IV.1 (Flux across SLCS). *Let* $\mathbf{z}$ *be a point on SLCS and* $\mathbf{j}^T(\mathbf{z}) = X(\mathbf{z}) \cdot \mathbf{n}(\mathbf{z})$*(amount of flux across SLCS at the point* $\mathbf{z}$*), and, then,* $\|\mathbf{j}^T(\mathbf{z})\| \leq \|X(\mathbf{z})\|\sin\alpha$.

Proof. The normal vector $\mathbf{n}(\mathbf{z})$ can be expanded in terms of $\xi_i^T(\mathbf{z})$ such as $\mathbf{n}(\mathbf{z}) = \sum_{i=1}^n a_i \xi_i^T(\mathbf{z})$. Then, $|a_n| = |\xi_n^T(\mathbf{z}) \cdot \mathbf{n}(\mathbf{z})| \geq \cos\alpha$ and $1 = \mathbf{n}(\mathbf{z}) \cdot \mathbf{n}(\mathbf{z}) = \sum_{i=1}^n a_i^2$ imply $\sqrt{\sum_{i=1}^{n-1} a_i^2} \leq \sin\alpha$. Under the condition A,

$$|X(\mathbf{z}) \cdot \mathbf{n}(\mathbf{z})| = \left|X(\mathbf{z}) \cdot \left(\mathbf{n}(\mathbf{z}) - a_n \xi_n^T(\mathbf{z})\right)\right|, \tag{10}$$

$$\leq \|X(\mathbf{z})\|\|\mathbf{n}(\mathbf{z}) - a_n \xi_n^T(\mathbf{z})\|, \tag{11}$$

$$= \|X(\mathbf{z})\| \sqrt{\sum_{i=1}^{n-1} a_i^2}, \tag{12}$$

$$\leq \|X(\mathbf{z})\|\sin\alpha. \tag{13}$$

□

Theorem IV.1 guarantees that the flux across an SLCS is as small as needed, provided that α is chosen small enough in the detection of the SLCS. In Sec. V, we investigate the relationship between SLCS and normally hyperbolic invariant hypersurfaces.

V. A CODIMENSION-ONE NHIM IS AN SLCS OVER LONG-ENOUGH TIME INTERVALS

Here, we show that a normally repelling inflowing-invariant manifold of codimension-one satisfies all conditions in the definition of a repelling SLCS for large enough times $T > 0$. We start by recalling the definition of an inflowing invariant manifold from Fenichel,[3] formulated for the specific case of codimension-one manifolds. We note that a similar relationship holds between codimension-one overflowing invariant manifolds and attracting SLCSs.

Let M be a C^r compact, codimension-one manifold with boundary ∂M, properly embedded in $\mathbb{R}^n$. Assume that M is inflowing invariant, i.e., X is tangent to M and X points strictly inwards on the boundary ∂M. Let us also assume that the manifold M is normally repelling, i.e., its normal repelling rate is larger than the largest rate of repulsion measured along M. This property can be expressed in terms of Lyapunov-type numbers introduced by Fenichel.[3] For the definition of Lyapunov-type numbers, along with more precise settings, see Appendix C. Our main result on the relationship between such NHIMs and SLCSs can be stated as follows.

Theorem V.1. *For large enough* $T > 0$*, any codimension-one normally repelling inflowing invariant manifold is a repelling SLCS in the sense of Definition IV.1. More precisely, the followings hold (for the explanation of the positive constants* $c_1, c_2, \hat{a}(<1), \hat{s}(<1)$*, see Appendix C).*

1. $$\sqrt{c_n^T(\mathbf{z})} > \hat{a}^{-T}\left(1 - c_1^{(1-\hat{s})} c_2 \hat{a}^{(1-\hat{s})T}\right)/c_1. \tag{14}$$

If T is chosen sufficiently large, the right hand side of Eq. (14) is greater than 1.

2. $$|L^T(\mathbf{z})| < \|X(\mathbf{z})\| \frac{\sqrt{2c_2 c_1^{(1-\hat{s})} \hat{a}^{(1-\hat{s})T}}}{1 - c_2 c_1^{(1-\hat{s})} \hat{a}^{(1-\hat{s})T}}, = O\left(\hat{a}^{(1-\hat{s})T}\right). \tag{15}$$

3. The tolerance ϵ can be chosen as

$$\epsilon = \frac{2c_2 c_1^{1-\hat{s}} \hat{a}^{(1-\hat{s})T}}{\left(1 + \sqrt{1 - 4c_1^{(1-\hat{s})} \hat{a}^{(1-\hat{s})T}}\right)\left(1 - c_1^{(1-\hat{s})} c_2 \hat{a}^{(1-\hat{s})T}\right)^{(1-\hat{s})}} = O\left(\hat{a}^{(1-\hat{s})T}\right), \tag{16}$$

and the tolerance α

$$\alpha = \cos^{-1}\left(1 - c_2 c_1^{(1-\hat{s})} \hat{a}^{(1-\hat{s})T}\right) \tag{17}$$

$$= O(\hat{a}^{(1-\hat{s})T/2}). \tag{18}$$

Proof. See Appendix C. □

VI. NUMERICAL DETECTION OF SLCSS

Based on Theorem V.1, we can closely approximate NHIMs using SLCSs through the following two simple steps:

1. Construct the zero level set of the function $L^T(\mathbf{z})$ defined in condition A of Definition IV.1.
2. Exclude parts of this zero level set that violate conditions B and C of Definition IV.1.

In carrying out the second step, we have to set values for the two parameters involved in B and C of Definition IV.1. Recall that the parameter ϵ controls the convergence of the eigenvector field $\xi_n^T(\mathbf{z})$ in the function $L^T(\mathbf{z})$, whereas the parameter α controls how close the normal direction of the SLCS is to $\xi_n^T(\mathbf{z})$. If these parameters are set to small values, the resulting SLCS is well-converged, almost normally repelling and almost invariant, but it is also likely to be a smaller set. This smaller set will typically increase in size if a longer detection interval T is used, as larger portions of the NHIM to be detected will qualify as SLCSs.

Note that evaluating conditions A–C of Definition IV.1 only requires computations that are local in the phase space variable $\mathbf{z}$. This makes the present algorithm highly parallelizable. The surface normal featured in condition C can be computed as the normalized gradient of $L^T(\mathbf{z})$ obtained from finite differencing. Once extracted, a repelling SLCS can be further refined by advection under the flow map in backward time. This is because a nearby codimension-one repelling NHIM will act as an attractor in backward time, and hence attract the SLCS at an exponential rate.

VII. APPLICATION

A. ABC flow

In this section, we demonstrate how codimension-one NHIMs can be detected as SLCSs in the classic ABC flow (cf. Arnold[12,13]). This flow, a solution of the steady Euler equation, has received attention for its non-integrability,[14] invariant tori and chaos.[15] Even though the ABC velocity field is laminar, it generates particle motions, whose complexity is often referred to as Lagrangian turbulence (for details, see Ref. 16).

Fluid particle motion under the ABC flow satisfies the differential equations

$$\frac{dx}{dt} = A\sin z + C\cos y, \tag{19}$$

$$\frac{dy}{dt} = B\sin x + A\cos z, \tag{20}$$

$$\frac{dz}{dt} = C\sin y + B\cos x, \tag{21}$$

where the parameters are set as $A=\sqrt{3}$, $B=\sqrt{2}$, and $C=1$, following Henon.[13] In this section, the position (x, y, z) is denoted by $\mathbf{z}$.

The system represented by Eqs. (19)–(21) is known to admit hyperbolic fixed points and hyperbolic periodic orbits. Subsets of the stable and unstable manifolds of hyperbolic periodic orbits are expected to be codimension-one (i.e., two-dimensional) NHIMs. In Fig. 2(a), we show periodic orbits revealed by less than 10 iterations of a Poincaré map. The largest absolute value of the corresponding Floquet exponent is indicated in color. A side view of the plot is shown in Fig. 2(b).

In Fig. 2(b), we show a few dominant hyperbolic periodic orbits with larger Floquet exponents in yellow color, which are indicated by blue squares in Fig. 2(a). The ABC flow is a volume-preserving three-dimensional system, and hence each unstable periodic orbit has three Floquet exponents, λ, 0, $-\lambda$, where $\lambda>0$ is the largest Floquet exponent. Accordingly, the Floquet exponent λ gives the ratio between normally repelling (contracting) rates and tangential repelling (contracting) rates of the stable (unstable) manifolds emanating from the periodic orbits. Therefore, the stable and unstable manifolds emanating from the periodic orbits indicated by blue squares have stronger normal hyperbolicity and hence are expected to dominate transport in phase space.

We now compute SLCSs to obtain a close approximation of the stable and unstable manifolds of the dominant periodic orbits of the ABC flow. We set the tolerance parameter ϵ to be 0.005. In terms of the Floquet exponent, this value corresponds to $-\ln(0.005)/10.0 \approx 0.5298$ and it is in between those of periodic orbits indicated by blue squares and those of the others (see Fig. 2). Contrastingly, the parameter α should be chosen in the same order as $\sqrt{\epsilon} \approx 0.0707$. It is because from Eqs. (16) and (18),

$$\alpha = O\left(\hat{a}^{\frac{1}{4}T\left(1-\sqrt{1-\frac{4\ln\epsilon}{T\ln\hat{a}}}\right)}\right), \tag{22}$$

$$\approx O\left(\hat{a}^{\frac{1}{4}T\left(1-1+\frac{2\ln\epsilon}{T\ln\hat{a}}\right)}\right), \tag{23}$$

$$= O\left(\hat{a}^{\frac{1}{2}\frac{\ln\epsilon}{\ln\hat{a}}}\right), \tag{24}$$

$$= O(\sqrt{\epsilon}). \tag{25}$$

In what follows, α is set to 0.05 for simplicity.

In Fig. 3, SLCS is plotted in the whole phase space $[0,2\pi]\times[0,2\pi]\times[0,2\pi]$. This SLCS is calculated as follows. First, we prepare $1200\times1200\times1200$ grids on the phase space $[0,2\pi]\times[0,2\pi]\times[0,2\pi]$ and calculate $L^T(\mathbf{z})$ for each grid. Here, T is set to $T=10$ (or $T=-10$), which corresponds to roughly the quadruple of the rotational period of the vortexes running through the phase space. The trajectories and their differentials are calculated by numerical integration of Eqs. (1) and (3). The numerical integration is done by using Stepper Dropper853,[17] which is 8-th order Runge-Kutta method with step size control. Double and quadruple precision were both tested in our numerical integration, producing almost identical results. Therefore, we conclude that double precision is sufficient for our purposes. To calculate $\xi_n^T(\mathbf{z})$, Singular Value Decomposition (SVD)[17] of $D\phi^T(\mathbf{z})$ is used. To identify the zero level set of $L^T(\mathbf{z})$, Marching Cube algorithm[18] is used. Specifically, one of the simplest variants of Marching Cube algorithms[19] that was originally developed by Doi.[20] The two tolerances α and ϵ are chosen as $\alpha=0.05$ and $\epsilon=0.005$. The results are plotted using ParaView,[21] version 3.14.

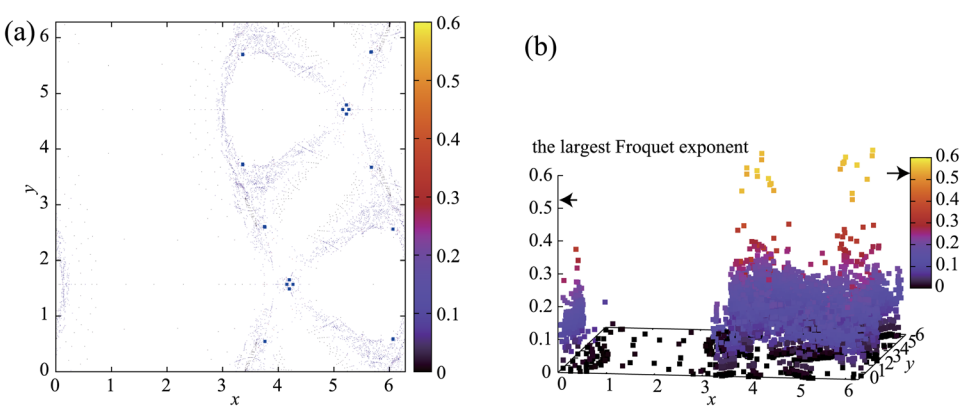

FIG. 2. (a) periodic orbits whose periods less than 10 iterations of the Poincaré map are plotted on the Poincaré surface $z=0$. The largest absolute value of the Floquet exponent of each periodic orbit is indicated by color (the periodic orbits that have the absolute value larger than 0.5 are indicated by blue squares). (b) A side view of (a). In (b), the value of the Floquet exponent 0.5298 that corresponds to $\epsilon=0.005$ is indicated by the arrows.

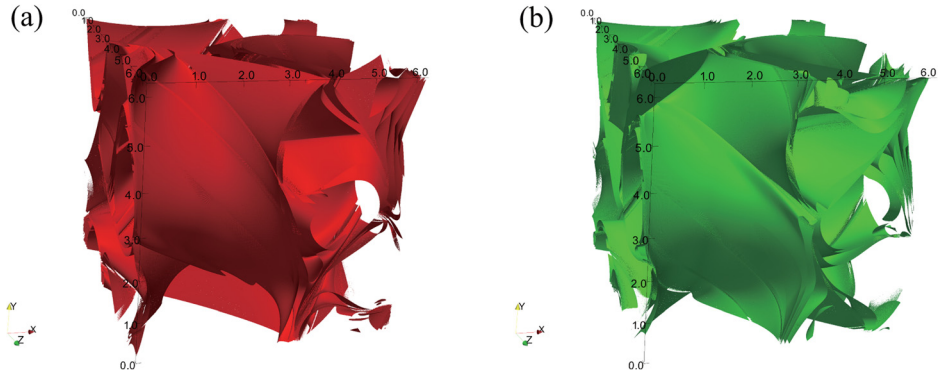

FIG. 3. (a), (b) SLCS $\mathcal{M}^T_{\epsilon,\alpha}$ plotted in the whole phase space ($T=10.0$ in red (a) and $T=-10.0$ in green (b), $\epsilon=0.005$, $\alpha=0.05$).

To take a closer look at them, in Fig. 4, SLCS is plotted on the Poincaré surface, where $z=0$ (it is equivalent to $z=2\pi$ surface due to the periodic boundary condition) and $x, y \in [0, 2\pi]$, in the same manner as before but by using $38\,400 \times 38\,400$ grids on the plane $[0, 2\pi] \times [0, 2\pi]$. The periodic orbits are plotted in the same surface and they are located at intersections between the two SLCSs indicated by red and green. If the SLCSs capture the stable/unstable manifolds of the periodic orbits, the periodic orbits should be located at the intersection between the two SLCSs. To investigate the relation the SLCSs and the stable and unstable manifolds, in Figs. 4(b) and 4(c), the local stable and unstable manifolds of two unstable period-3 periodic orbits are superposed on Fig. 4(a). In Figs. 4(b) and 4(c), the unstable periodic orbits are indicated by blue squares and the local stable manifolds by cyan bold line and the local unstable manifolds by pink bold line.

These lines coincide with some lines of the SLCSs. To investigate the relation between the SLCSs and the stable and unstable manifolds more clearly, in Fig. 4(d), the magnified figure in the vicinity of one of the periodic points, located at (5.15972, 4.71239), are shown, along with the local stable and unstable manifolds are superposed on it, where the local stable and unstable manifolds are indicated by cyan and pink, respectively. In Fig. 4, the deviation between SLCSs and the local stable and unstable manifolds are of order 1.0×10^{-3}, which is of the same order as ϵ (Note that ϵ corresponds to the convergence tolerance of $L^T(\mathbf{z})$ with respect to T, see Eq. (9)).

VIII. SUMMARY

We have introduced a new technique for the global detection of codimension-one normally hyperbolic invariant

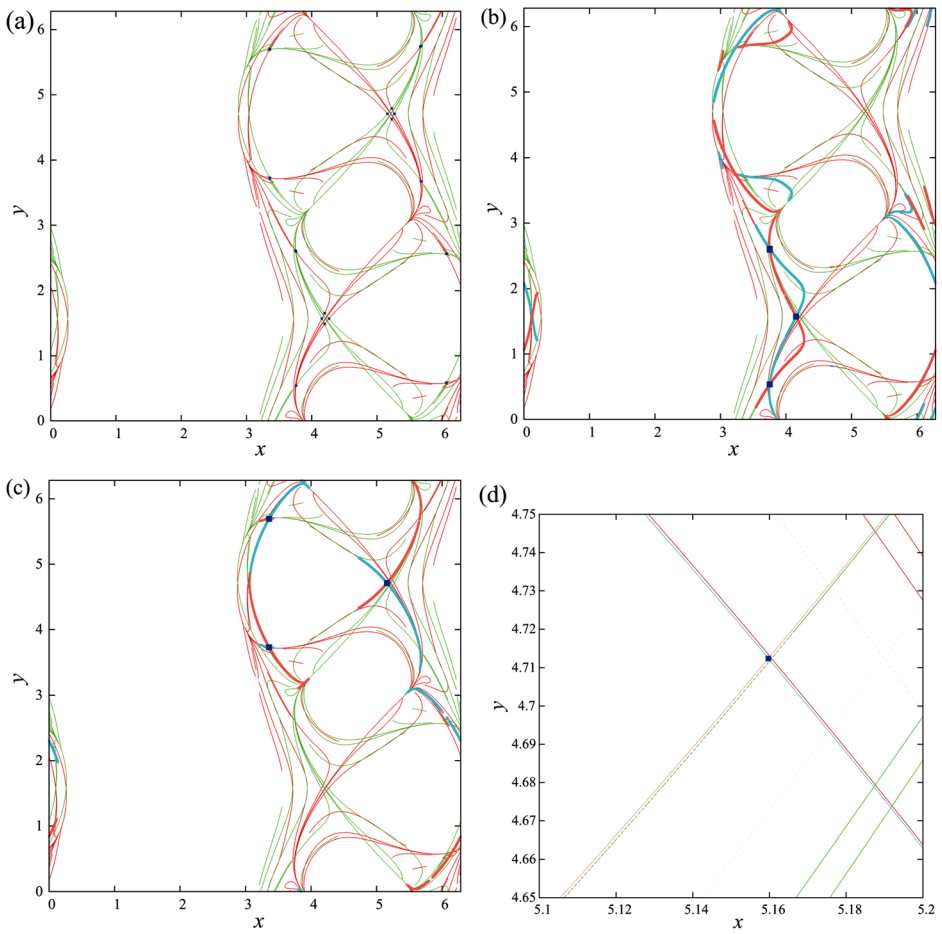

FIG. 4. (a) SLCS $\mathcal{M}^T_{\epsilon,\alpha}$ plotted on the Poincaré surface $z=0$ ($T=10.0$ in red and $T=-10.0$ in green, $\epsilon=0.005$, $\alpha=0.05$). The periodic orbits indicated by blue squares in Fig. 2 are plotted on the surface. (b), (c) the local stable and unstable manifolds of the two period-3 periodic orbits (indicated by blue squares) are superposed on (a). The local stable and unstable manifolds are indicated by cyan and pink, respectively. (d) a magnified figure of (c).

manifolds in finite-dimensional autonomous dynamical systems. The detection is achieved through the identification of Stationary Lagrangian Coherent Structures (SLCSs), which are codimension-one quasi-invariant surfaces satisfying simple necessary conditions for being an LCS over a finite time interval of length T.

As a first step, we locate zero level set of the inner product of the vector field defining the dynamical system with the dominant eigenvector of the Cauchy-Green strain tensor, with the latter tensor computed from the time T flow map. As a second step, parts of this zero level set are eliminated either because they are not normally repelling (or attracting) enough, or because they are too far from being invariant. These two elimination steps are precisely controlled through the choice of two small parameters involved in the definition of the SLCS. The approximation of NHIMs through SLCSs can be further refined by advecting the extracted SLCSs in the time direction in which they are attracting. This zero set necessarily contains all LCSs by the variational theory of Haller[10] and, Farazmand and Haller,[11] as well as by the recent geodesic theory of transport barriers developed by Haller and Beron-Vera.[22]

Using the classic ABC flow as an example, we have shown how this SLCS detection reveals the stable and unstable manifolds of periodic orbits with high accuracy. Remarkably, our technique requires no *a priori* information on the location of the underlying periodic orbits, their stability types, or their Floquet multipliers. This feature distinguishes our technique from available numerical NHIM detection methods that invariably assume some *a priori* knowledge[6] or a first guess about the invariant manifold to be detected.[7,8]

Several powerful methods exist for computing stable and unstable manifolds of specifically known invariant sets, such as fixed pints and periodic orbits.[23] The present paper provides a general approach that identifies influential manifolds all over the phase space, without the need to know the asymptotic behavior of the trajectories in the manifold. Even if periodic orbits are known to exist, their accurate numerical detection can pose a challenge.[24,25] Errors in locating periodic orbits in turn translate to even larger errors in computing their stable and unstable manifolds. Thus our approach offers an advantage in this case as well, as it does not need the precise location of a periodic orbit in order to compute its stable or unstable manifolds.

To apply our approach to discretized data sets, interpolations are needed to approximate the underlying smooth vector field. The quality of the interpolation depends on the degree of smoothness of this vector field, as well as the type and density of the grid on which the data set is given. All these factors make it difficult to provide a general assessment of the numerical errors arising in the automated detection of NHIMs as stationary LCSs. By the persistence theorem of NHIMs,[3] however, as long as we manage to keep the errors of our numerical procedures small, the manifold we construct is C^r close to the corresponding NHIM in the underlying smooth vector field.

While the present approach is generally applicable to arbitrary finite-dimensional autonomous dynamical systems, its direct extension to non-autonomous dynamical systems is not straightforward. This is because instantaneous snapshots of a time-dependent NHIM are generally far from being invariant, and hence the underlying non-autonomous vector field defining the dynamical system is generally not tangent to the NHIM. For this reason, an extension of our approach to detecting non-autonomous invariant manifolds (i.e., invariant manifolds in an extended phase space) requires further ideas and will be pursued elsewhere.

ACKNOWLEDGMENTS

T.H. would like to thank Professor Mikito Toda, Professor Zin Arai, Dr. Kristjan Onu, Mr. Mohammad Farazmand, Mr. Hossein Kafiabad, Mr. Brendan Keith, and Mr. Preetom Nag, for valuable comments. This work has been supported by JSPS, the Cooperative Research Program of "Network Joint Research Center for Materials and Devices", Research Center for Computational Science, Okazaki, Japan, and Priority Area "Molecular Theory for Real Systems" (to T.K.), Grant-in-Aid for Young Scientists (B) (to T.H.), Grant-in-Aid for challenging Exploratory Research (to T.K.), and Grant-in-Aid for Scientific Research (B) (to T.K.) from the Ministry of Education, Culture, Sports, Science and Technology, the Office of the President of Hokkaido University through a priority distribution fund for research support (to T.H.) and the Canadian NSERC under Grant No. 401839-11 (to G.H.).

APPENDIX A: EVALUATION OF THE T DERIVATIVE OF $\xi_n^T(\mathbf{z})$

Here, we provide a proof of Eq. (7). First, note that the matrix $D\phi^T(\mathbf{z})(D\phi^T(\mathbf{z}))^*$ has the same eigenvalues as the Cauchy-Green strain tensor. Let $\eta_i^T(\mathbf{z})\,(i=1,\ldots,n)$ be an eigenvector corresponding to $c_i^T(\mathbf{z})\,(i=1,\ldots,n)$ such that $\eta_i^T(\mathbf{z})\cdot\eta_j^T(\mathbf{z})=\delta_{ij}\,(i,j=1,\ldots,n)$ and $D\phi^T(\mathbf{z})\xi_i^T(\mathbf{z})=\sqrt{c_i^T(\mathbf{z})}\eta_i^T(\mathbf{z})\,(i=1,\ldots,n)$. In terms of these eigenvalues and eigenvectors, $\frac{d\xi_i^T(\mathbf{z})}{dT}$ can be evaluated as

$$\frac{d\xi_i^T(\mathbf{z})}{dT}=\sum_{j\neq i}\frac{1}{c_i^T(\mathbf{z})-c_j^T(\mathbf{z})}\left[\xi_j^T(\mathbf{z})^*\frac{dC^T(\mathbf{z})}{dT}\xi_i^T(\mathbf{z})\right]\xi_j^T(\mathbf{z}), \tag{A1}$$

where

$$\begin{aligned}
&\xi_j^T(\mathbf{z})^*\frac{dC^T(\mathbf{z})}{dT}\xi_i^T(\mathbf{z})\\
&=\xi_j^T(\mathbf{z})^*\frac{d}{dT}\left(D\phi^T(\mathbf{z})\right)^*D\phi^T(\mathbf{z})\xi_i^T(\mathbf{z})\\
&\quad+\xi_j^T(\mathbf{z})^*\left(D\phi^T(\mathbf{z})\right)^*\frac{d}{dT}D\phi^T(\mathbf{z})\xi_i^T(\mathbf{z}),\\
&=\xi_j^T(\mathbf{z})^*\left(D\phi^T(\mathbf{z})\right)^*\frac{\partial X(\mathbf{z}')^*}{\partial\mathbf{z}'}D\phi^T(\mathbf{z})\xi_i^T(\mathbf{z})\\
&\quad+\xi_j^T(\mathbf{z})^*\left(D\phi^T(\mathbf{z})\right)^*\frac{\partial X(\mathbf{z}')}{\partial\mathbf{z}'}D\phi^T(\mathbf{z})\xi_i^T(\mathbf{z}),\\
&=\sqrt{c_j^T(\mathbf{z})c_i^T(\mathbf{z})}\eta_j^T(\mathbf{z})^*\left(\frac{\partial X(\mathbf{z}')^*}{\partial\mathbf{z}'}+\frac{\partial X(\mathbf{z}')}{\partial\mathbf{z}'}\right)\eta_i^T(\mathbf{z})
\end{aligned} \tag{A2}$$

($\mathbf{z}'=\phi^T(\mathbf{z})$). Equation (A1) can be derived by differentiating $C^T(\mathbf{z})\xi_i^T(\mathbf{z})=c_i^T(\mathbf{z})\xi_i^T(\mathbf{z})\,(i=1,\ldots,n)\,(c_1^T(\mathbf{z})\leq c_2^T(\mathbf{z})\leq\cdots\leq c_n^T(\mathbf{z}))$, with respect to T as follows:

$$\frac{dC^T(\mathbf{z})}{dT}\xi_i^T(\mathbf{z}) + C^T(\mathbf{z})\frac{d\xi_i^T(\mathbf{z})}{dT} = \frac{dc_i^T(\mathbf{z})}{dT}\xi_i^T(\mathbf{z}) + c_i^T(\mathbf{z})\frac{d\xi_i^T(\mathbf{z})}{dT}. \quad \text{(A3)}$$

By calculating the innerproduct between this vector and $\xi_j^T(\mathbf{z})$,

$$\xi_j^T(\mathbf{z})^*\frac{dC^T(\mathbf{z})}{dT}\xi_i^T(\mathbf{z}) + c_j^T(\mathbf{z})\xi_j^T(\mathbf{z})^*\frac{d\xi_i^T(\mathbf{z})}{dT} = \frac{dc_i^T(\mathbf{z})}{dT}\delta_{ij} + c_i^T(\mathbf{z})\xi_j^T(\mathbf{z})^*\frac{d\xi_i^T(\mathbf{z})}{dT}, \quad \text{(A4)}$$

and, then,

$$\xi_j^T(\mathbf{z})^*\frac{d\xi_i^T(\mathbf{z})}{dT} = \frac{1}{c_i^T(\mathbf{z}) - c_j^T(\mathbf{z})} \times \left[\xi_j^T(\mathbf{z})^*\frac{dC^T(\mathbf{z})}{dT}\xi_i^T(\mathbf{z}) - \frac{dc_i^T(\mathbf{z})}{dT}\delta_{ij}\right]. \quad \text{(A5)}$$

Note that $\xi_i^T(\mathbf{z})^*\frac{d\xi_i^T(\mathbf{z})}{dT} = 0\,(i = 1, \ldots, n)$ because $\frac{d}{dT}(\xi_i^T(\mathbf{z})^*\xi_i^T(\mathbf{z})) = \frac{d\delta_{ii}}{dT} = 0$. The conjunction of this relation and Eq. (A5) results in Eq. (A1).

Using Eqs. (A1) and (A2), the magnitude of $\frac{d\xi_n^T(\mathbf{z})}{dT}$ can be evaluated as follows:

$$\left\|\frac{d\xi_n^T(\mathbf{z})}{dT}\right\| = \left\|\sum_{j\neq n}\frac{1}{c_n^T(\mathbf{z}) - c_j^T(\mathbf{z})} \times \left[\xi_j^T(\mathbf{z})^*\frac{dC^T(\mathbf{z})}{dT}\xi_n^T(\mathbf{z})\right]\xi_j^T(\mathbf{z})\right\|, \quad \text{(A6)}$$

$$\leq \frac{1}{c_n^T(\mathbf{z}) - c_{n-1}^T(\mathbf{z})}\left\|\sum_{j\neq n}\left[\xi_j^T(\mathbf{z})^*\frac{dC^T(\mathbf{z})}{dT}\xi_n^T(\mathbf{z})\right]\xi_j^T(\mathbf{z})\right\|, \quad \text{(A7)}$$

$$= \frac{1}{c_n^T(\mathbf{z}) - c_{n-1}^T(\mathbf{z})} \times \sqrt{\sum_{j\neq n}\left[\xi_j^T(\mathbf{z})^*\frac{dC^T(\mathbf{z})}{dT}\xi_n^T(\mathbf{z})\right]^2}, \quad \text{(A8)}$$

$$= \frac{1}{c_n^T(\mathbf{z}) - c_{n-1}^T(\mathbf{z})} \times \sqrt{\sum_{j\neq n} c_n^T(\mathbf{z})c_j^T(\mathbf{z})\left[\eta_j^T(\mathbf{z})^*\left(\frac{\partial X(\mathbf{z}')^*}{\partial \mathbf{z}'} + \frac{\partial X(\mathbf{z}')}{\partial \mathbf{z}'}\right)\eta_n^T(\mathbf{z})\right]^2}, \quad \text{(A9)}$$

$$\leq \frac{1}{c_n^T(\mathbf{z}) - c_{n-1}^T(\mathbf{z})}\sqrt{c_n^T(\mathbf{z})c_{n-1}^T(\mathbf{z})} \times \sqrt{\sum_{j\neq n}\left[\eta_j^T(\mathbf{z})^*\left(\frac{\partial X(\mathbf{z}')^*}{\partial \mathbf{z}'} + \frac{\partial X(\mathbf{z}')}{\partial \mathbf{z}'}\right)\eta_n^T(\mathbf{z})\right]^2}, \quad \text{(A10)}$$

$$\leq \frac{\sqrt{c_n^T(\mathbf{z})c_{n-1}^T(\mathbf{z})}}{c_n^T(\mathbf{z}) - c_{n-1}^T(\mathbf{z})}\sqrt{\sum_{j\neq n}\left\|\frac{\partial X(\mathbf{z}')^*}{\partial \mathbf{z}'} + \frac{\partial X(\mathbf{z}')}{\partial \mathbf{z}'}\right\|^2}, \quad \text{(A11)}$$

$$= \frac{\sqrt{c_n^T(\mathbf{z})c_{n-1}^T(\mathbf{z})}}{c_n^T(\mathbf{z}) - c_{n-1}^T(\mathbf{z})}\sqrt{n-1}\left\|\frac{\partial X(\mathbf{z}')^*}{\partial \mathbf{z}'} + \frac{\partial X(\mathbf{z}')}{\partial \mathbf{z}'}\right\|, \quad \text{(A12)}$$

$$\leq \frac{\sqrt{c_{n-1}^T(\mathbf{z})/c_n^T(\mathbf{z})}}{1 - c_{n-1}^T(\mathbf{z})/c_n^T(\mathbf{z})}\sqrt{n-1}G, \quad \text{(A13)}$$

where G is defined in Eq. (8) and $\mathbf{z}' = \phi^T(\mathbf{z})$. If $c_{n-1}^T(\mathbf{z})/c_n^T(\mathbf{z}) < \epsilon^2$, we have $\|\frac{d\xi_n^T(\mathbf{z})}{dT}\| < \frac{\sqrt{n-1}G\epsilon}{1-\epsilon^2}$.

APPENDIX B: A SIMPLE EXAMPLE OF A STABLE MANIFOLD THAT IS NOT LCS

Let

$$\frac{dx}{dt} = -x, \quad \text{(B1)}$$

$$\frac{dy}{dt} = y + y^2, \quad \text{(B2)}$$

be an ordinary differential equation defined on $\mathbf{R}^2$. This system admits a solution

$$\phi^T(x,y) = \left(xe^{-T}, \frac{ye^T}{1 + y(1 - e^T)}\right). \quad \text{(B3)}$$

Its differential and the other variables are

$$D\phi^T(x,y) = \begin{pmatrix} e^{-T} & 0 \\ 0 & \frac{e^T}{\left(1 + y(1 - e^T)\right)^2} \end{pmatrix}, \quad \text{(B4)}$$

$$c_1^T(x,y) = e^{-2T}, \quad \text{(B5)}$$

$$c_2^T(x,y) = \frac{e^{2T}}{\left(1 + y(1 - e^T)\right)^4}, \quad \text{(B6)}$$

and

$$\xi_1^T(x,y) = (1,0), \quad \text{(B7)}$$

$$\xi_2^T(x,y) = (0,1). \quad \text{(B8)}$$

$Y = 0$ is a stable manifold of this system and it is tangent to $\xi_1^T(x,y)$ but

$$\xi_2^T(x,0)\cdot\nabla c_2^T(x,0) = 4e^{2T}(1 - e^T) \neq 0 \quad \text{(B9)}$$

for all T. Therefore, this stable manifold satisfies the condition III, whereas it does not satisfy the condition IV. This example indicates that stable manifolds are not necessarily LCSs.

APPENDIX C: PROOF OF THEOREM V.1

1. Precise setting of Theorem V.1

Let $\bar{M} = M \cup \partial M$ be a C^r, $n-1$ dimensional, compact, connected manifold that is properly embedded in $\mathbb{R}^n$ and inflowing invariant under X. In terms of the Euclidean metric

in $\mathbb{R}^n$, $T\mathbb{R}^n|_M$ ($\supset TM$) splits into $T\mathbb{R}^n|_M = TM \oplus N$ where N is the bundle of vectors normal to TM. Let $\pi : T\mathbb{R}^n|_M \to N$ be the orthogonal projection to N along TM. Note that $\dim(\mathrm{Im}\,\pi) = \dim(N_{\mathbf{z}}) = 1$ for all $\mathbf{z} \in M$. In terms of the normal vector to M, $\mathbf{n}(\mathbf{z})$ ($\|\mathbf{n}(\mathbf{z})\| = 1$), the orthogonal projection of $v \in T_{\mathbf{z}}\mathbb{R}^n|_M$ to $N_{\mathbf{z}}$ can be written as $\pi v \equiv (\mathbf{n}(\mathbf{z}) \cdot v)\mathbf{n}(\mathbf{z})$. Let $A^t(\mathbf{z}) = D\phi^t(\mathbf{z})|_{T_{\mathbf{z}}M}$ and $B^t(\mathbf{z}) = \pi D\phi^{-t}(\phi^t(\mathbf{z}))$. A schematic figure to explain the two operators is shown in Fig. 5.

In terms of $A^t(\mathbf{z})$ and $B^t(\mathbf{z})$, Lyapunov types number $\nu(\mathbf{z})$ and $\sigma(\mathbf{z})$ can be defined as $\nu(\mathbf{z}) = \inf\{a | \|B^t(\mathbf{z})\|/a^t \to 0, \text{as } t \to \infty\}$ and $\sigma(\mathbf{z}) = \inf\{s | \|A^t(\mathbf{z})\|\|B^t(\mathbf{z})\|^s \to 0, \text{as } t \to \infty\}$, where $\|B^t(\mathbf{z})\| = \sup_{v \in T_{\phi^t(\mathbf{z})}\mathbb{R}^n} \frac{\|B^t(\mathbf{z})v\|}{\|v\|}$ and $\|A^t(\mathbf{z})\| = \sup_{v \in T_{\mathbf{z}}M} \frac{\|A^t(\mathbf{z})v\|}{\|v\|}$. Suppose $\nu(z) < 1$ and $\sigma(\mathbf{z}) < 1$ for all $\mathbf{z} \in M$. The condition $\nu(\mathbf{z}) < 1$ corresponds to the situation that, at the point $\mathbf{z}$, maximum stretching rate normal to M grows exponentially fast as $t \to \infty$. The second condition $\sigma(\mathbf{z}) < 1$ corresponds to the situation that the stretching rate normal to M dominates over that tangential to M. Note that the condition $\nu(\mathbf{z}) < 1$ does not depend on the choice of the metric. In addition, if $\nu(\mathbf{z}) < 1$ holds, then the condition $\sigma(\mathbf{z}) < 1$ does not depend on the choice of the metric, either.[3] Let M be a manifold that satisfies the above properties.

2. Proof of Theorem V.1

By using the uniformity lemma,[3] the Lyapunov types numbers $\nu(\mathbf{z})$ and $\sigma(\mathbf{z})$ attain their suprema on M, thus, $\sup_{\mathbf{z}\in M} \nu(\mathbf{z}) < 1$ and $\sup_{\mathbf{z}\in M} \sigma(\mathbf{z}) < 1$. Then, there are real constants $c_1, c_2 > 0$, $\hat{a} < \sup_{\mathbf{z}\in M} \nu(\mathbf{z})$ and $\hat{s} < \sup_{\mathbf{z}\in M} \sigma(\mathbf{z})$ such that

$$\|B^t(\mathbf{z})\| < c_1 \hat{a}^t, \tag{C1}$$

and

$$\|A^t(\mathbf{z})\|\|B^t(\mathbf{z})\|^{\hat{s}} < c_2, \tag{C2}$$

for all $t > 0$ and $\mathbf{z} \in M$.

Proof of Eq. (14): Note that the matrix $D\phi^T(\mathbf{z})(D\phi^T(\mathbf{z}))^*$ has the same eigenvalues as $C^T(\mathbf{z})$, which are $c_1^T(\mathbf{z}), \ldots, c_n^T(\mathbf{z})$. Let $\eta_i^T(\mathbf{z})$ be an eigenvector that corresponds to $c_i^T(\mathbf{z})$ such that $\sqrt{c_i^T(\mathbf{z})}\eta_i^T(\mathbf{z}) = D\phi^T(\mathbf{z})\xi_i^T(\mathbf{z})$ $(i = 1, \ldots, n)$ and $\eta_i^T(\mathbf{z}) \cdot \eta_j^T(\mathbf{z}) = \delta_{ij}$ (For the relationship between the two sets of eigenvectors $\xi_i^T(\mathbf{z})$ and $\eta_i^T(\mathbf{z})$, see Ref. 17). Since $D\phi^{-T}(\phi^T(\mathbf{z})) = D\phi^T(\mathbf{z})^{-1}$, $D\phi^{-T}(\phi^T(\mathbf{z}))\eta_i^T(\mathbf{z}) = \xi_i^T(\mathbf{z})/\sqrt{c_i^T(\mathbf{z})}$ $(i = 1, \ldots, n)$. By using this fact,

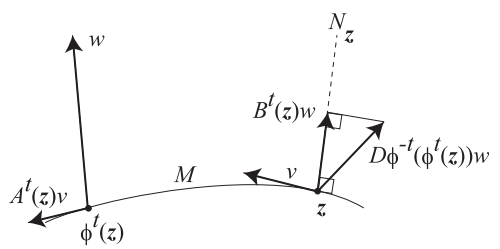

FIG. 5. A schematic figure to explain the two operators $A^t(\mathbf{z})$ and $B^t(\mathbf{z})$.

$$\|B^T(\mathbf{z})\| \geq \|\pi\xi_n^T(\mathbf{z})\|/\sqrt{c_n^T(\mathbf{z})}. \tag{C3}$$

It is because

$$\|B^T(\mathbf{z})\| = \sup_{v \in T_{\phi^T(\mathbf{z})}\mathbb{R}^n} \frac{\|B^T(\mathbf{z})v\|}{\|v\|}, \tag{C4}$$

$$\geq \frac{\|B^T(\mathbf{z})\eta_n^T(\mathbf{z})\|}{\|\eta_n^T(\mathbf{z})\|}, \tag{C5}$$

$$= \|B^T(\mathbf{z})\eta_n^T(\mathbf{z})\|, \tag{C6}$$

$$= \|\pi D\phi^{-T}\left(\phi^T(\mathbf{z})\right)\eta_n^T(\mathbf{z})\|, \tag{C7}$$

$$= \|\pi\xi_n^T(\mathbf{z})\|/\sqrt{c_n^T(\mathbf{z})}. \tag{C8}$$

Next,

$$\sqrt{c_n^T(\mathbf{z})}\left(1 - \|\pi\xi_n^T(\mathbf{z})\|\right) \leq \|A^T(\mathbf{z})\| \tag{C9}$$

is shown as follows. This inequality follows from the following two inequalities:

$$\|D\phi^T(\mathbf{z})(1-\pi)\xi_n^T(\mathbf{z})\| \leq \|A^T(\mathbf{z})\|, \tag{C10}$$

and

$$\sqrt{c_n^T(\mathbf{z})}\left(1 - \|\pi\xi_n^T(\mathbf{z})\|\right) \leq \|D\phi^T(\mathbf{z})(1-\pi)\xi_n^T(\mathbf{z})\|. \tag{C11}$$

Equation (C10) follows immediately from the fact $(1-\pi)\xi_n^T(\mathbf{z}) \in T_{\mathbf{z}}M$ because

$$\begin{aligned}\|D\phi^T(\mathbf{z})(1-\pi)\xi_n^T(\mathbf{z})\| &= \|A^T(\mathbf{z})(1-\pi)\xi_n^T(\mathbf{z})\|,\\ &\leq \|A^T(\mathbf{z})\|\|(1-\pi)\xi_n^T(\mathbf{z})\|,\\ &\leq \|A^T(\mathbf{z})\|,\end{aligned} \tag{C12}$$

where the last inequality comes from the fact that $1-\pi$ is the orthogonal projection to TM along N, $\|(1-\pi)\xi_n^T(\mathbf{z})\|^2 + \|\pi\xi_n^T(\mathbf{z})\|^2 = \|\xi_n^T(\mathbf{z})\|^2 = 1$, resulting in $\|(1-\pi)\xi_n^T(\mathbf{z})\| \leq \|\xi_n^T(\mathbf{z})\| = 1$.

Equation (C11) can be proved as follows:

$$\|D\phi^T(\mathbf{z})(1-\pi)\xi_n^T(\mathbf{z})\| = \|D\phi^T(\mathbf{z})\xi_n^T(\mathbf{z}) - D\phi^T(\mathbf{z})\pi\,\xi_n^T(\mathbf{z})\|, \tag{C13}$$

$$= \|\sqrt{c_n^T(\mathbf{z})}\eta_n^T(\mathbf{z}) - D\phi^T(\mathbf{z})\pi\,\xi_n^T(\mathbf{z})\|, \tag{C14}$$

$$\geq \|\sqrt{c_n^T(\mathbf{z})}\eta_n^T(\mathbf{z})\| - \|D\phi^T(\mathbf{z})\pi\,\xi_n^T(\mathbf{z})\|, \tag{C15}$$

$$\geq \sqrt{c_n^T(\mathbf{z})}\|\eta_n^T(\mathbf{z})\| - \|D\phi^T(\mathbf{z})\|\|\pi\,\xi_n^T(\mathbf{z})\|, \tag{C16}$$

$$\geq \sqrt{c_n^T(\mathbf{z})}\left(1 - \|\pi\,\xi_n^T(\mathbf{z})\|\right). \tag{C17}$$

Using Eqs. (C3) and (C9),

$$\left(1 - \sqrt{c_n^T(\mathbf{z})}\|B^T(\mathbf{z})\|\right)\sqrt{c_n^T(\mathbf{z})} \leq \|A^T(\mathbf{z})\|. \tag{C18}$$

Combining this inequality with Eq. (C2),

$$\left(1-\sqrt{c_n^T(\mathbf{z})}\|B^T(\mathbf{z})\|\right)\sqrt{c_n^T(\mathbf{z})}\|B^T(\mathbf{z})\| < c_2\|B^T(\mathbf{z})\|^{1-\hat{s}}. \tag{C19}$$

Note that,

$$1 = \|\pi\|, \tag{C20}$$

$$= \|\pi\left(D\phi^T(\mathbf{z})\right)^{-1}D\phi^T(\mathbf{z})\|, \tag{C21}$$

$$= \|\pi D\phi^{-T}\left(\phi^T(\mathbf{z})\right)D\phi^T(\mathbf{z})\|, \tag{C22}$$

$$= \|B^T(\mathbf{z})D\phi^T(\mathbf{z})\|, \tag{C23}$$

$$\le \|B^T(\mathbf{z})\|\|D\phi^T(\mathbf{z})\|, \tag{C24}$$

$$= \|B^T(\mathbf{z})\|\sqrt{c_n^T(\mathbf{z})}. \tag{C25}$$

Here, the last equality holds due to Eqs. (5) and (6). Equation (C19) conjunction with Eq. (C25) results in

$$\left(1-\sqrt{c_n^T(\mathbf{z})}\|B^T(\mathbf{z})\|\right) < c_2\|B^T(\mathbf{z})\|^{1-\hat{s}}. \tag{C26}$$

Using Eqs. (C1) and (C26), $c_n^T(\mathbf{z})$ can be evaluated from below, such as

$$\sqrt{c_n^T(\mathbf{z})} > \hat{a}^{-T}\left(1-c_1^{(1-\hat{s})}c_2\hat{a}^{(1-\hat{s})T}\right)/c_1. \tag{C27}$$

Proof of Eq. (18): Noting that $\|\pi\xi_n^T(\mathbf{z})\| = |\mathbf{n}(\mathbf{z})\cdot\xi_n^T(\mathbf{z})|$, $\|\pi\xi_n^T(\mathbf{z})\|$ can be evaluated as follows. Starting from Eq. (C9) and using Eq. (C2), Eq. (C3) and $\|\pi\xi_n^T(\mathbf{z})\| \le 1$,

$$\left(1-\|\pi\xi_n^T(\mathbf{z})\|\right) \le \frac{\|A^T(\mathbf{z})\|}{\sqrt{c_n^T(\mathbf{z})}}, \tag{C28}$$

$$\le \|A^T(\mathbf{z})\|\|B^T(\mathbf{z})\|, \tag{C29}$$

$$< c_2\|B^T(\mathbf{z})\|^{(1-\hat{s})}. \tag{C30}$$

Using Eq. (C1), Eq. (C30) results in $\left(1-\|\pi\xi_n^T(\mathbf{z})\|\right) < c_2c_1^{(1-\hat{s})}\hat{a}^{(1-\hat{s})T}$ and therefore

$$1-c_2c_1^{(1-\hat{s})}\hat{a}^{(1-\hat{s})T} < \|\pi\xi_n^T(\mathbf{z})\| \tag{C31}$$

holds. Since $\|\pi\xi_n^T(\mathbf{z})\| = |\mathbf{n}(\mathbf{z})\cdot\xi_n^T(\mathbf{z})| = \cos\alpha$, Eq. (C31) implies Eq. (18).

Proof of Eq. (16): If

$$\sqrt{\frac{c_j^T(\mathbf{z})}{c_n^T(\mathbf{z})^{\hat{s}}}} < \frac{c_2}{\frac{1}{2}\left(1+\sqrt{1-4c_1^{(1-\hat{s})}\hat{a}^{(1-\hat{s})T}}\right)}, \tag{C32}$$

for $j = 1,\ldots,n-1$ is shown, Eq. (16) immediately follows by multiplying $\|B^T(\mathbf{z})\|^{(1-\hat{s})}$ to both sides of Eq. (C32)

$$\sqrt{\frac{c_j^T(\mathbf{z})}{c_n^T(\mathbf{z})^{\hat{s}}}}\|B^T(\mathbf{z})\|^{(1-\hat{s})} < \frac{c_2}{\frac{1}{2}\left(1+\sqrt{1-4c_1^{(1-\hat{s})}\hat{a}^{(1-\hat{s})T}}\right)} \times \|B^T(\mathbf{z})\|^{(1-\hat{s})}, \tag{C33}$$

$$\sqrt{\frac{c_j^T(\mathbf{z})}{c_n^T(\mathbf{z})^{\hat{s}}}}\frac{\|\pi\xi_n^T(\mathbf{z})\|^{(1-\hat{s})}}{\sqrt{c_n^T(\mathbf{z})}^{(1-\hat{s})}} < \frac{c_2}{\frac{1}{2}\left(1+\sqrt{1-4c_1^{(1-\hat{s})}\hat{a}^{(1-\hat{s})T}}\right)} \times c_1^{(1-\hat{s})}\hat{a}^{(1-\hat{s})T}, \tag{C34}$$

$$\sqrt{\frac{c_j^T(\mathbf{z})}{c_n^T(\mathbf{z})}} < \frac{c_2}{\frac{1}{2}\left(1+\sqrt{1-4c_1^{(1-\hat{s})}\hat{a}^{(1-\hat{s})T}}\right)} \times c_1^{(1-\hat{s})}\hat{a}^{(1-\hat{s})T}/\|\pi\xi_n^T(\mathbf{z})\|^{(1-\hat{s})}, \tag{C35}$$

$$\sqrt{\frac{c_j^T(\mathbf{z})}{c_n^T(\mathbf{z})}} < \frac{c_2}{\frac{1}{2}\left(1+\sqrt{1-4c_1^{(1-\hat{s})}\hat{a}^{(1-\hat{s})T}}\right)} \times \frac{c_1^{(1-\hat{s})}\hat{a}^{(1-\hat{s})T}}{\left(1-c_2c_1^{(1-\hat{s})}\hat{a}^{(1-\hat{s})T}\right)^{(1-\hat{s})}}, \tag{C36}$$

from Eqs. (C1),(C8) and (C31).

Let $j \in \{1,\ldots,n-1\}$. To show Eq. (C32),

$$\sqrt{c_j^T(\mathbf{z})} \le \frac{\|A^T(\mathbf{z})\|}{|\xi_j^T(\mathbf{z})\cdot(1-\pi)\xi_j^T(\mathbf{z})|}, \tag{C37}$$

and

$$|\xi_j^T(\mathbf{z})\cdot\pi\xi_j^T(\mathbf{z})| \le \sqrt{c_j^T(\mathbf{z})}\|B^T(\mathbf{z})\| \tag{C38}$$

are used (the proofs will be given later). Combining Eqs. (C37) and (C38) with Eqs. (C1), (C2), and $0 < \hat{s} < 1$,

$$|\xi_j^T(\mathbf{z})\cdot\pi\,\xi_j^T(\mathbf{z})||\xi_j^T(\mathbf{z})\cdot(1-\pi)\xi_j^T(\mathbf{z})| \le \|A^T(\mathbf{z})\|\|B^T(\mathbf{z})\|, \tag{C39}$$

and

$$|\xi_j^T(\mathbf{z})\cdot\pi\,\xi_j^T(\mathbf{z})|\left(1-|\xi_j^T(\mathbf{z})\cdot\pi\xi_j^T(\mathbf{z})|\right) < c_2c_1^{(1-\hat{s})}\hat{a}^{(1-\hat{s})T}. \tag{C40}$$

The right hand side of Eq. (C40) goes to 0 as $T\to\infty$, and, therefore, either $|\xi_j^T(\mathbf{z})\cdot\pi\xi_j^T(\mathbf{z})| \to 0$ or $|\xi_j^T(\mathbf{z})\cdot\pi\xi_j^T(\mathbf{z})| \to 1$. The latter case contradicts with the fact that $\xi_j^T(\mathbf{z})$ and $\xi_n^T(\mathbf{z})$ are mutually orthogonal with each other. Since $\|\xi_j^T(\mathbf{z})\| = 1$ $(j = 1,\ldots,n)$, there are subsequences $T_1 < T_2 < \cdots$ such that the limits $\tilde{\xi}_n(\mathbf{z}) = \lim_{i\to\infty}\xi_n^{T_i}(\mathbf{z})$ and $\tilde{\xi}_j(\mathbf{z}) = \lim_{i\to\infty}\xi_j^{T_i}(\mathbf{z})$ exist. Since Eq. (C31) ensures $\|\pi\tilde{\xi}_n(\mathbf{z})\| = 1$, $\mathbf{n}(\mathbf{z})$ and $\tilde{\xi}_n(\mathbf{z})$ are parallel, i.e., $\mathbf{n}(\mathbf{z}) \parallel \tilde{\xi}_n(\mathbf{z})$. On the other hand, the latter case $|\tilde{\xi}_j(\mathbf{z})\cdot\pi\tilde{\xi}_j(\mathbf{z})| = 1$ results in $\|\pi\tilde{\xi}_j(\mathbf{z})\| = 1$, which means $1 = \|\pi\tilde{\xi}_j(\mathbf{z})\| = |\mathbf{n}(\mathbf{z})\cdot\tilde{\xi}_j(\mathbf{z})| = |\tilde{\xi}_n(\mathbf{z})\cdot\tilde{\xi}_j(\mathbf{z})|$. This contradicts the fact that $\tilde{\xi}_j(\mathbf{z})$ and $\tilde{\xi}_n(\mathbf{z})$ are orthogonal. Therefore, $|\xi_j^T(\mathbf{z})\cdot\pi\xi_j^T(\mathbf{z})| \to 0$ as $T\to\infty$. Using Eq. (C40), the convergence rate can be evaluated as

$$|\xi_j^T(\mathbf{z})\cdot\pi\xi_j^T(\mathbf{z})|<\frac{1}{2}\left(1-\sqrt{1-4c_1^{(1-\hat{s})}\hat{a}^{(1-\hat{s})T}}\right). \quad \text{(C41)}$$

Using this inequality, Eqs. (C2), (C25) and (C37),

$$\sqrt{\frac{c_j^T(\mathbf{z})}{c_n^T(\mathbf{z})^{\hat{s}}}}\le\frac{\|A^T(\mathbf{z})\|\|B^T(\mathbf{z})\|^{\hat{s}}}{|\xi_j^T(\mathbf{z})\cdot(1-\pi)\xi_j^T(\mathbf{z})|}, \quad \text{(C42)}$$

$$<\frac{c_2}{1-|\xi_j^T(\mathbf{z})\cdot\pi\xi_j^T(\mathbf{z})|}, \quad \text{(C43)}$$

$$<\frac{c_2}{\frac{1}{2}\left(1+\sqrt{1-4c_1^{(1-\hat{s})}\hat{a}^{(1-\hat{s})T}}\right)}. \quad \text{(C44)}$$

Finally let us prove Eqs. (C37) and (C38) as follows. Let $j\in\{1,\cdots,n\}$. Because $D\phi^T(\mathbf{z})\xi_j^T(\mathbf{z})=\sqrt{c_j^T(\mathbf{z})}\eta_j^T(\mathbf{z})$, we have

$$\begin{aligned}&|\eta_j^T(\mathbf{z})\cdot D\phi^T(\mathbf{z})(1-\pi)\xi_j^T(\mathbf{z})|\\&=|\xi_j^T(\mathbf{z})\cdot(1-\pi)\xi_j^T(\mathbf{z})|\sqrt{c_j^T(\mathbf{z})}.\end{aligned} \quad \text{(C45)}$$

Contrastingly,

$$|\eta_j^T(\mathbf{z})\cdot D\phi^T(\mathbf{z})(1-\pi)\xi_j^T(\mathbf{z})| \quad \text{(C46)}$$

$$\le\|D\phi^T(\mathbf{z})(1-\pi)\xi_j^T(\mathbf{z})\|, \quad \text{(C47)}$$

$$=\|A^T(\mathbf{z})(1-\pi)\xi_j^T(\mathbf{z})\|, \quad \text{(C48)}$$

$$\le\|A^T(\mathbf{z})\|\|(1-\pi)\xi_j^T(\mathbf{z})\|, \quad \text{(C49)}$$

where the second equality follows because $A^T(\mathbf{z})=D\phi^T(\mathbf{z})|_{T_\mathbf{z}M}$ and $1-\pi$ is the orthogonal projection to $T_\mathbf{z}M$ along $N_\mathbf{z}$. The above two equations end up with Eq. (C37)

$$|\xi_j^T(\mathbf{z})\cdot B^T(\mathbf{z})\eta_j^T(\mathbf{z})| \quad \text{(C50)}$$

$$=|\xi_j^T(\mathbf{z})\cdot\pi D\phi^{-T}\left(\phi^T(\mathbf{z})\right)\eta_j^T(\mathbf{z})|, \quad \text{(C51)}$$

$$=|\xi_j^T(\mathbf{z})\cdot\pi\xi_j^T(\mathbf{z})|/\sqrt{c_j^T(\mathbf{z})}. \quad \text{(C52)}$$

Moreover,

$$|\xi_j^T(\mathbf{z})\cdot B^T(\mathbf{z})\eta_j^T(\mathbf{z})|\le\|B^T(\mathbf{z})\eta_j^T(\mathbf{z})\|, \quad \text{(C53)}$$

$$=\|B^T(\mathbf{z})\|. \quad \text{(C54)}$$

These two equations result in Eq. (C38).

Proof of Eq. (C15)*:* $X(\mathbf{z})$ can be expanded with respect to $\xi_i^T(\mathbf{z})\,(i=1,\ldots,n)$ as $X(\mathbf{z})=\sum_{i=1}^n(\xi_i^T(\mathbf{z})\cdot X(\mathbf{z}))\xi_i^T(\mathbf{z})$. Note that $\pi X(\mathbf{z})=0$. Then,

$$0=\pi\sum_{i=1}^n\left(\xi_i^T(\mathbf{z})\cdot X(\mathbf{z})\right)\xi_i^T(\mathbf{z})=\sum_{i=1}^n\left(\xi_i^T(\mathbf{z})\cdot X(\mathbf{z})\right)\pi\xi_i^T(\mathbf{z}). \quad \text{(C55)}$$

Using this,

$$\left(\xi_n^T(\mathbf{z})\cdot X(\mathbf{z})\right)\pi\xi_n^T(\mathbf{z})=-\sum_{j=1}^{n-1}\left(\xi_j^T(\mathbf{z})\cdot X(\mathbf{z})\right)\pi\xi_j^T(\mathbf{z}), \quad \text{(C56)}$$

holds and its norm can be evaluated as

$$|\xi_n^T(\mathbf{z})\cdot X(\mathbf{z})|\|\pi\xi_n^T(\mathbf{z})\| \quad \text{(C57)}$$

$$=\|-\sum_{j=1}^{n-1}\left(\xi_j^T(\mathbf{z})\cdot X(\mathbf{z})\right)\pi\xi_j^T(\mathbf{z})\|, \quad \text{(C58)}$$

$$\le\sqrt{\sum_{j=1}^{n-1}|\xi_j^T(\mathbf{z})\cdot X(\mathbf{z})|^2}\sqrt{\sum_{j=1}^{n-1}\|\pi\xi_j^T(\mathbf{z})\|^2}, \quad \text{(C59)}$$

$$\le\|X(\mathbf{z})\|\sqrt{\sum_{j=1}^{n-1}\|\pi\xi_j^T(\mathbf{z})\|^2}. \quad \text{(C60)}$$

If T is taken sufficiently large, the left hand side of $1-c_2c_1^{(1-\hat{s})}\hat{a}^{(1-\hat{s})T}\le\|\pi\xi_n^T(\mathbf{z})\|$ becomes nonzero. Therefore,

$$|\xi_n^T(\mathbf{z})\cdot X(\mathbf{z})|\le\frac{\|X(\mathbf{z})\|\sqrt{\sum_{j=1}^{n-1}\|\pi\xi_j^T(\mathbf{z})\|^2}}{\|\pi\xi_n^T(\mathbf{z})\|}, \quad \text{(C61)}$$

$$\le\|X(\mathbf{z})\|\frac{\sqrt{\sum_{j=1}^{n-1}\|\pi\xi_j^T(\mathbf{z})\|^2}}{1-c_2c_1^{(1-\hat{s})}\hat{a}^{(1-\hat{s})T}}. \quad \text{(C62)}$$

If $\sqrt{\sum_{j=1}^{n-1}\|\pi\xi_j^T(\mathbf{z})\|^2}$ can be evaluated from above, this proof is done. Note that $\|\pi\xi_j^T(\mathbf{z})\|=|\mathbf{n}(\mathbf{z})\cdot\xi_j^T(\mathbf{z})|\,(1\le j\le n)$ and $1=|\mathbf{n}(\mathbf{z})\cdot\mathbf{n}(\mathbf{z})|=\sum_{j=1}^n|\mathbf{n}(\mathbf{z})\cdot\xi_j^T(\mathbf{z})|^2$. This is because $\xi_j^T(\mathbf{z})\,(1\le j\le n)$ is an orthonormal basis and $\mathbf{n}(\mathbf{z})$ can be expanded as $\mathbf{n}(\mathbf{z})=\sum_{j=1}^n(\xi_j^T(\mathbf{z})\cdot\mathbf{n}(\mathbf{z}))\xi_j^T(\mathbf{z})$. By these identities, $1-\|\pi\xi_n^T(\mathbf{z})\|^2=\sum_{j=1}^{n-1}\|\pi\xi_j^T(\mathbf{z})\|^2$. Using Eq. (C31), we obtain

$$\sum_{j=1}^{n-1}\|\xi_j^T(\mathbf{z})\|^2=1-\|\pi\xi_n^T(\mathbf{z})\|^2 \quad \text{(C63)}$$

$$=\left(1-\|\pi\xi_n^T(\mathbf{z})\|\right)\left(1+\|\pi\xi_n^T(\mathbf{z})\|\right) \quad \text{(C64)}$$

$$\le2\left(1-\|\pi\xi_n^T(\mathbf{z})\|\right) \quad \text{(C65)}$$

$$<2c_2c_1^{(1-\hat{s})}\hat{a}^{(1-\hat{s})T}. \quad \text{(C66)}$$

By combining Eqs. (C60) and (C66), we obtain

$$|\xi_n^T(\mathbf{z})\cdot X(\mathbf{z})|<\|X(\mathbf{z})\|\frac{\sqrt{2c_2c_1^{(1-\hat{s})}\hat{a}^{(1-\hat{s})T}}}{1-c_2c_1^{(1-\hat{s})}\hat{a}^{(1-\hat{s})T}}. \quad \text{(C67)}$$

[1]M. W. Hirsch, C. C. Pugh, and M. Shub, "Invariant manifolds," Bull. Am. Math. Soc. **76**, 1015 (1970).
[2]M. W. Hirsch, C. C. Pugh, and M. Shub, *Invariant Manifolds, Volume 583 of Lecture Notes in Mathematics* (Springer-Verlag, Berlin, 1977).
[3]N. Fenichel, "Persistence and smoothness of invariant manifolds for flows," Indiana Univ. Math. J. **21**, 193 (1971).
[4]S. Wiggins, *Normally Hyperbolic Invariant Manifolds in Dynamical Systems* (Springer, New York, 1994).
[5]C. K. T. J. Jones, "Geometric singular perturbation theory," in *Dynamical Systems Montecatini, Terme, Lect. Notes. Math.* (Springer-Verlag, 1994).
[6]G. Haller, *Chaos Near Resonance* (Springer, 1999).
[7]H. W. Broer, A. Hagen, and G. Begter, "Numerical continuation of normally hyperbolic invariant manifolds," Nonlinearity **20**, 1499 (2007).
[8]M. J. Capinski and C. Simó, "Computer assisted proof for normally hyperbolic invariant manifolds," Nonlinearity **25**, 1997 (2012).
[9]G. Haller and G.-C. Yuan, "Lagrangian coherent structure and mixing in two-dimensional turbulence," Physica D **147**, 352 (2000).
[10]G. Haller, "A variational theory of hyperbolic lagrangian coherent structures," Physica D **240**, 574 (2011).
[11]M. Farazmand and G. Haller, "Computing Lagrangian Coherent Strucures from variational LCS theory," Chaos **22**, 013128 (2012).
[12]V. I. Arnold, "Sur la topologie des ecoulemenets stationnaires des fluides parfaits," C. R. Acad. Sci. Paris **261**, 17 (1965).
[13]M. M. Hénon, "Sur la topologie des lignes de courant dans un cas particulier," C. R. Acad. Sci. Paris **262**, 312 (1966).
[14]A. J. Maciejewski and M. Przybylska, "Non-integrability of abc flow," Phys. Lett. **303**, 265 (2002).
[15]X.-H. Zhao, D.-B. Huang, and H.-H. Dai, "Invatiant tori and chaotic streamlines in the abc flow," Phys. Lett. **237**, 136 (1998).
[16]T. Dombre, U. Frisch, J. M. Greene, M. Hénon, A. Mehr, and A. M.Soward, "Chaotic streamlines in the abc flows," J. Fluid Mech. **167**, 353 (1986).
[17]W. H. Press, S. A. Teukolosky, W. T. Vetterling, and B. P. Flannery, *Numerical Recipes, The Art of Scientific Computing, International Series of Monographs on Chemistry*, 3rd ed. (Cambridge University Press, 2007).
[18]T. S. Newman and H. Yi, "A survey of the marching cubes algorithm," Comput. Graphics **30**, 854 (2006).
[19]A. Guéziec and R. Hummel, "Exploiting triangulated surface extraction using tetrahedral decomposition," IEEE Trans. Visual. Comput. Graph. **1**, 328 (1995).
[20]A. Doi and A. Koide, "An efficient method of triangulating equi-valued surfaces by using tetrahedral cells," IEICE Trans. E**74**, 214 (1991).
[21]J. Ahrens, B. Geveci, and C. Law, "ParaView: An End-User Tool for Large Data Visualization," in *The Visualization Handbook*, edited by C. Hansen and C. Johnson (Academic Press, 2005), p. 717.
[22]G. Haller and F. J. Beron-Vera, "Geodesic theory of transport barriers in two-dimensional flows," Physica D **241**, 1680 (2012).
[23]B. Krauskopf, H. M. Osinga, E. J. Doedel, M. E. Henderson, J. Guckenheimer, A. Vladimirsky, M. Dellnitz, and O. Junge, "A survey of methods for computing (un)stable manifolds of vector fields," Chaos Appl. Sci. Eng. **15**, 763 (2005).
[24]Z. Galias and W. Tucker, "Rigorous study of short periodic orbits for the lorenz system," *ISCAS, IEEE*, p. 764, 2008.
[25]A. Katok and B. Hasselblatt, *Introduction to the Modern Theory of Dynamical Systems* (Cambridge University Press, New York, 2005).